ACS APPLIED MATERIALS & INTERFACES

Letter

www.acsami.org

Continuous Production of Janus and Composite Liquid Marbles with Tunable Coverage

Jasmine O. Castro, Bruna M. Neves, Amgad R. Rezk,* Nicky Eshtiaghi,* and Leslie Y. Yeo

School of Engineering, RMIT University, Melbourne, Victoria 3001, Australia

ABSTRACT: We report a simple method for on-demand continuous processing of composite liquid marbles with the aid of a 3D printed slide platform, which offers the potential for engineering novel functional surfaces for the production of combination drug therapies, particle-based barcode biomarkers and smart membranes, among other applications. Unlike other attempts at producing such liquid marbles, this novel technique not only facilitates controllable and reproducible production of the liquid marbles but also allows the selection of different morphologies such as banded, patchy, and Janus structures by controlling the coalescence conditions, with the possibility for tunable symmetric and asymmetric patterns, the latter by varying the particle species partitioning ratio.

KEYWORDS: *Janus, liquid marble, 3D printing, magnetic field, splitting, coalescence*

Liquid marbles are droplets comprising organic/inorganic liquids or even liquid metals, encapsulated by a coating of micron to nanometer sized hydrophobic or hydrophilic particles such as silica beads or natural powders like soot or *Lycopodium*.[1,2] The particle coating endows the liquid marble with a unique nonwetting and partial solidlike property,[3] which isolates it with an air cushion pocket from the underlying solid support, therefore not only offering opportunities for exploring novel and intriguing physics[4,5] but also allowing these entities to be exploited for a host of applications. In particular, its low adhesion and viscous drag makes it especially useful as a simple but versatile platform for discrete microfluidic droplet actuation and as an alternative approach to superhydrophobic surfaces. Other uses of liquid marbles have also been explored, such as its adoption as a miniature reactor/bioreactor,[6−8] micropump,[9] and gas/liquid sensor,[10,11] among others.[12]

Janus liquid marbles—liquid marbles partitioned with separate hemispherical domains comprising two different types of particles—have also been reported,[13] which allow their precise manipulation and actuation using external forces such as electric[13] or magnetic[14] fields in addition to serving as a template for engineering novel functional surfaces as vehicles for combination drug powder therapies,[15] particle barcodes that serve as biomarkers for multimodal imaging and diagnostics,[16] and smart membrane fabrics in next generation water harvesting, desalination, and fuel cell technologies.[17] The method for producing these Janus liquid marbles, although simple—merely by forcing two liquid marbles with different particle coatings to collide and hence coalesce[13]—does not facilitate appreciable control over its particle topology and morphology.

In this work, we demonstrate a simple process for rapid and continuous production of composite (Janus and other patterns, as described subsequently) liquid marbles that allows control over the ratio of the particle coverage as well as its morphology, thus facilitating some degree of tunability and reproducibility of its physicochemical properties. Given its simplicity and low cost, this process can easily be parallelised and automated for high throughput production. Although a technique to control the relative coverage between two liquids that comprise a Janus emulsion has been reported,[18] this cannot be extended to afford the same control over the particle coat partitioning in Janus liquid marbles; neither have other methods been proposed to date to achieve this, to the best of our knowledge.

The setup is schematically depicted in Figure 1 and consists of a 3D printed slide with ramps on both sides that guide droplets introduced from both sides at the top of the slide such that they converge at a constriction or orifice at the bottom of the slide (see, for example, the magnified image in the inset of Figure 1d). The side and front views of the 3D computer-aided design (AutoCAD 2015, AutoDesk Inc., San Rafael, CA) model are shown in Figure 1a, b, respectively, and images of the resulting construct produced using a 3D printer (MakerBot Replicator, MakerBot Industries LLC, Brooklyn, NY) are shown in Figure 1c. To generate the composite liquid marbles, we coat both ramp surfaces with a superhydrophobic material (NeverWet, NeverWet LLC, Lancaster, PA) and a section (3 mm in length) with different powders such that the droplets (10 μL deionized water, although the working fluid and volume can be adjusted depending on the liquid marble that is desired to be produced), when successively dispensed from the top of the slide from both sides, initially accelerates as it rolls down the slide along both ramps and are subsequently coated with the particles, thus forming liquid marbles of a specific particle coating during their descent. In practice, any particulate matter can be employed though we demonstrate the concept in this work using *Lycopodium* powder (50 nm, Sigma-Aldrich) as the

Received: May 6, 2016
Accepted: July 7, 2016
Published: July 7, 2016

DOI: 10.1021/acsami.6b05321
ACS Appl. Mater. Interfaces 2016, 8, 17751−17756

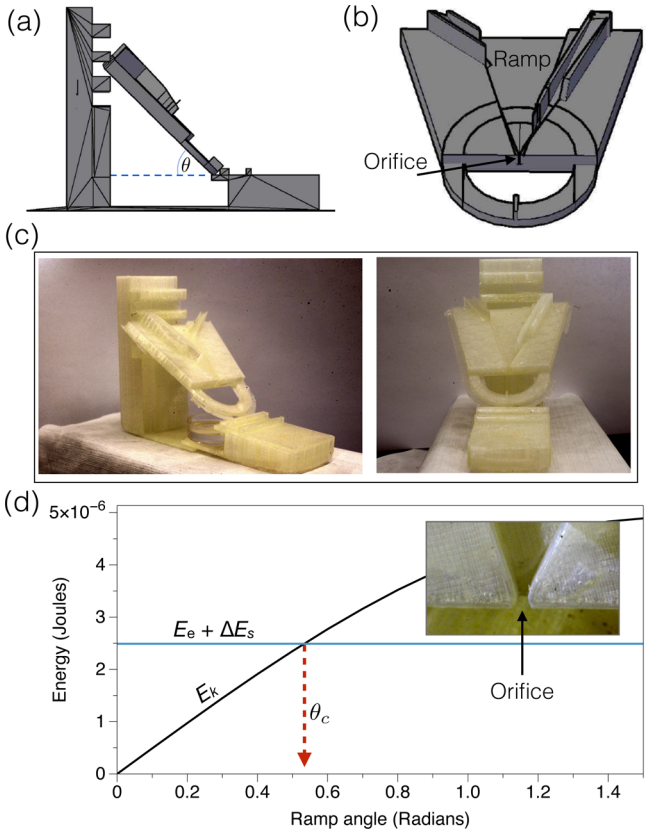

Figure 1. (a) Side view AutoCAD model of the experimental platform used for the continuous production of the composite liquid marbles, (b) angled magnified view taken above its slide section, and, (c) images of the actual 3D printed construction. (d) Kinetic E_k, elastic E_e, and surface E_s energy of the liquid marble as a function of the slide inclination angle θ showing the critical value θ_c at which the coalescence event transitions from one that occurs at the slide orifice due to trapping of the first liquid marble ($E_k < E_e + \Delta E_s$) to one that occurs after both liquid marbles traverse through the orifice ($E_k > E_e + \Delta E_s$). The inset shows a magnification of the orifice region at the bottom of the slide where the liquid marbles are trapped.

first particulate species and a 1:20 mixture of dyed *Lycopodium* powder and iron oxide particles (Fe_2O_3; 30 nm) as the second species. In the latter, pure *Lycopodium* powder is mixed with methyl violet and water at 1% concentration, followed by sonication for 2 min and subsequent heating at 120 °C for 30 min. The reason we employ the *Lycopodium*−iron oxide mixture as the second particulate species was to avoid the formation of clumps on the droplet surface that was observed when pure iron oxide was used. All materials were sourced from Sigma-Aldrich Pty. Ltd. (Castle Hill, NSW, Australia).

By judicious design of the inclination angle of the slide as well as the neck width of the orifice gap, two scenarios are then possible for the controlled coalescence between the two liquid marble species (i.e., pure *Lycopodium* and *Lycopodium*−iron oxide mix). At inclination angles below a critical value (Figure 2, left column), the first *Lycopodium* liquid marble produced as it rolls down the ramp (step 1) is trapped at the orifice (step 2)—designed to be slightly narrower than the liquid marble diameter (for the 10 μL droplets initially dispensed in the present experiments, which correspond to a diameter D of 1.7 mm, we set the orifice width to be 1.4 mm; besides the initial droplet volume, other parameters such as the roughness and the droplet velocity, which, in turn, is dependent on the inclination angle, are also factors to be accounted for when setting this width)—until the second *Lycopodium*−iron oxide liquid marble, produced when a second water droplet is dispensed and rolls down the right ramp (step 3), collides and hence coalesces with it (step 4). The momentum arising from the collision then causes the resultant composite liquid marble to squeeze through and dislodge from the orifice, where it drops into either a collection fluid (silicone oil, 1085 mPa.s; Cannon Instrument Co., State College, PA) housed in a Petri dish (Figure 2c-i) or onto a flat substrate (Figure 2c-ii). In contrast, above the critical inclination angle (Figure 2, right column), the first liquid marble has sufficient velocity and momentum as it rolls down the incline along the ramp such that it squeezes through the orifice without being trapped (steps 1 and 2), dropping into the collection fluid (Figure 2c-iii). This is also true of the second liquid marble, and thus the coalescence event is delayed until it drops into the collection fluid and lands over the first liquid marble and subsequently coalesces with it (Figure 2c-iv) to form the composite liquid marble.

The velocity and hence momentum of the droplets (or liquid marbles) as they roll along the ramps down the slide is therefore the crucial factor in determining the critical inclination angle of the slide that delineates the two coalescence scenarios, which, in turn, dictates the fate of the composite liquid marble. For the liquid marble to avoid being trapped at the orifice (i.e., the transition from the first to the second scenarios), it has to possess adequate kinetic energy E_k during its traverse down the incline to overcome the sum of its elastic energy E_e and the change in surface energy ΔE_s, such that it is able to deform sufficiently to squeeze through the orifice gap. Given the dispensed droplet rapidly accelerates due to the initial superhydrophobic section along the ramp, it is not unreasonable to assume that it reaches terminal velocity v by the time it reaches the orifice. If frictional losses are negligible

$$v(\theta) = (2gL\sin\theta)^{1/2} \tag{1}$$

from which the kinetic energy of the liquid marble

$$E_k(\theta) = mv^2/2 \tag{2}$$

can be calculated. Here, m is the mass of the liquid marble, g the gravitational acceleration, L the length of the slide, and θ its inclination. The elastic energy stored in the liquid marble, on the other hand, can be estimated by[19]

$$E_e = Gh(\xi/R_s)^2 S \tag{3}$$

wherein h and R_s are the thickness and radius of the liquid marble shell, respectively, the former being equivalent to the diameter of the coating particles d and the latter approximated by the droplet diameter D. ξ is the radial deformation of the liquid marble and S its area of contact with the solid, which we estimate to be the area that the liquid marble contacts with the solid surface around the orifice. G is the elastic modulus of the liquid marble shell, which can be approximated by

$$G = \frac{1-\nu}{1+\varphi}\frac{\gamma_e}{d} \tag{4}$$

in which $\nu \approx 0.5$ is the Poisson ratio, $\gamma_e \approx 60$ mN·m the effective surface tension of the liquid marble, and $\varphi = 0.68$ the maximum hard sphere packing fraction. To calculate the change in surface energy ΔE_s, we assume that the initially spherical liquid marble of diameter D deforms into a prolate spheroid whose semiaxis

DOI: 10.1021/acsami.6b05321
ACS Appl. Mater. Interfaces 2016, 8, 17751−17756

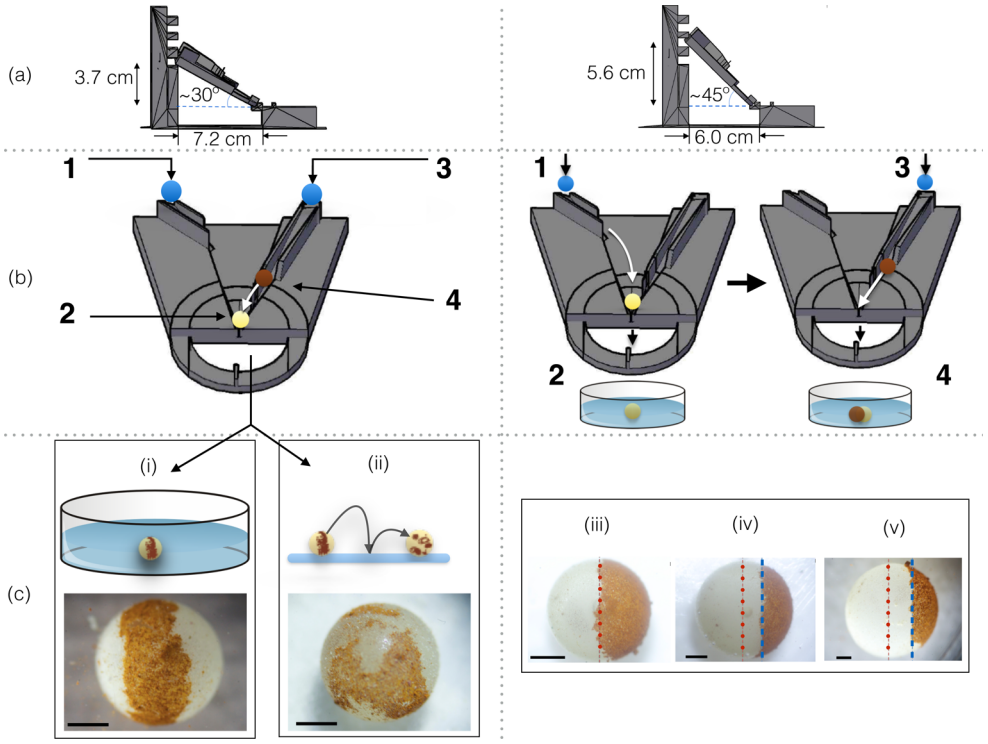

Figure 2. Effect of the slide inclination angle (left column: $\theta = 30° < \theta_c$; right column: $\theta = 45° > \theta_c$) on the formation of the composite liquid marble. (a) Side and (b) front view CAD rendering of the slide showing the trajectory of the droplet during its transition into a liquid marble and subsequent coalescence with its second counterpart to form a composite marble. Step 1: The first water droplet is dispensed from the top of the slide and rolls down the ramp where it picks up the particles (*Lycopodium*) coated on the ramp surface to form the first liquid marble. Step 2: If the inclination angle is below a critical value (left column: $\theta = 30° < \theta_c$), the first liquid marble does not gain sufficient velocity and hence momentum during its descent to be able to squeeze through the orifice and is trapped at this position. If, however, the inclination angle surpasses the critical value (right column: $\theta = 45° > \theta_c$), the first liquid marble manages to squeeze through the orifice and drops into the collection fluid. Step 3: A second water droplet is dispensed from the top of the slide and forms the second liquid marble as it is coated with particles (*Lycopodium*−iron oxide mix) during its descent. Step 4: If $\theta = 30° < \theta_c$ (left column), it collides and coalesces with the first liquid marble trapped at the orifice to form a composite liquid marble; because of the collision, there is sufficient momentum for the composite marble to squeeze through the orifice to fall into the collection dish or plate. If $\theta = 45° > \theta_c$ (right column), the second liquid marble follows the fate of the first liquid marble in squeezing through the orifice to fall into the collection fluid, where it coalesces with the first liquid marble to form the composite marble. (c) Formation of the composite liquid marble. For $\theta = 30° < \theta_c$ (left column), the coalescence occurs rapidly at the slide orifice and the composite marble is subsequently released. (i) If the composite marble falls into a collection dish filled with oil, it forms a banded structure. If, on the other hand, it falls onto a solid surface (ii), the band is dispersed and a patchy structure culminates. For $\theta = 45° > \theta_c$ (right column), the coalescence occurs slowly in the collection fluid to produce (iii) a symmetric (1:1) Janus liquid marble. Further adding a third and fourth *Lycopodium* liquid marble, on the other hand, allows the species partitioning to be tuned, resulting in asymmetric Janus liquid marbles with (iv) 1:2 and (v) 1:3 ratios. The dotted red lines in these images represent the actual centerline indicating a theoretical 1:1 split, whereas the dashed blue lines in (iv) and (v) represent the theoretical 1:2 and 1:3 splits, showing good agreement with that obtained experimentally. The theoretical splits were obtained from a calculation of the surface areas based on the ratio between the corresponding volumes of each of the liquid droplets added to form the Janus liquid marble. The scale bars denote a length of approximately 1 mm.

length a is equivalent to the orifice dimension; the other semiaxis dimension b can then be obtained from volume conservation, i.e., $b = D^3/8a^2$. The change in surface energy can then be computed from

$$\Delta E_s = \gamma_e(A_{s_2} - A_{s_1}) \tag{5}$$

where A_{s_1} is the surface area of the initially undeformed sphere and A_{s_2} is that of the prolate spheroid. Figure 1d shows the energies computed from eqs 2, 3, and 5, thus allowing the critical transition angle $\theta_c \approx 31°$ to be estimated from the crossover.

This prediction of the critical angle is close to that experimentally observed, which from Figure 2, lies between 30° and 45°. Where and how the coalescence event occurs between the first *Lycopodium* and second *Lycopodium*−iron oxide liquid marbles is dependent on whether the slide inclination is below or above this critical value, and, more importantly, is observed to determine the fate of the composite liquid marble that is produced. For $\theta = 30° < \theta_c$ (Figure 2, left column) where the coalescence occurs rapidly at the slide orifice and results in the formation of a composite marble at this location before being squeezed out as a consequence of the momentum gained from the collision and falling into the collector, two further scenarios are possible. If the composite marble drops into an oil bath, a band of rust colored *Lycopodium*−iron oxide particles is trapped between two white *Lycopodium* hemispherical caps (Figure 2c-i). Although this structure resembles the so-called "watermelon" structure reported by Bormashenko et al.,[13] those appear to have been produced serendipitously rather than by judicious design; however, in the present case, we are able to reproducibly produce these structures in a controllable manner. The mechanism by which this occurs is as follows: When the

DOI: 10.1021/acsami.6b05321
ACS Appl. Mater. Interfaces 2016, 8, 17751−17756

composite liquid marble lands on the solid surface, it first deforms into a pancakelike shape because of inertial impact but subsequently retracts under the action of capillary forces and bounces off the surface. The bouncing continues until the potential/kinetic energy is progressively dissipated by the viscous force and surface friction. As a consequence of the bouncing, the uniform coverage of the loosely packed *Lycopodium*−iron oxide particle coating is disrupted and breaks up into patches.

A likely mechanism by which such a structure forms is illustrated in Figure 3. Upon collision and coalescence with the

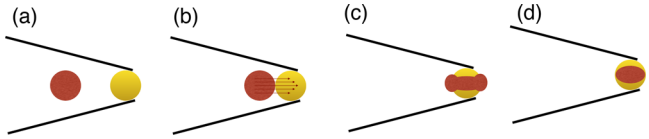

Figure 3. (a−d) Schematic illustration of a possible mechanism that is responsible for the formation of the banded liquid marble.

first liquid marble that is immobilized at the orifice, the momentum from the second liquid marble drives an internal flow in the merged liquid marble along the longitudinal axis in the direction of the collision. The sidewalls of the orifice, however, retard this flow such that a parabolic-like velocity profile arises within the merged marble. The strong velocity along the centerline then drives the *Lycopodium*−iron oxide particles from the rear section, which originated from the second liquid marble, to displace the *Lycopodium* particles in the front section, which originated from the first liquid marble, along the longitudinal axis. Given the retardation of the flow due to the no-slip condition imposed by the sidewalls of the orifice, there is little flow on either sides of the merged marble adjacent to the walls and hence the *Lycopodium* particles are not displaced by the *Lycopodium*−iron oxide particles. A banded structure then results when the marble regains its spherical shape once it is released from the orifice trap. Figure 2c-ii, on the other hand, shows that a hard landing scenario in which the composite marble falls onto a solid surface results in the dispersion of the particle band to produce a random patchy liquid marble.

For $\theta = 45° > \theta_c$ (Figure 2, right column), the coalescence between the two liquid marbles produced on the slide occurs, in contrast, slowly in the collection fluid when the second liquid marble drops into the oil bath where the first marble has landed, as exemplified in Figure 4a, b. Coalescence thus ensues (Figures 4c, d) if the velocity of the second liquid marble exceeds the critical coalescence velocity

$$u_c \approx \left(\frac{\gamma_e}{\rho D}\right)^{1/2}\left(\frac{d/D}{2+\kappa D}\right)^{1/4} \quad (6)$$

which has been derived based on the criterion that coalescence only occurs if the impact results in the deformation of the liquid marbles to an extent such that the curvatures of their interfaces, which are on the order of the inverse capillary length $\kappa = (\rho g/\gamma_e)^{1/2}$ in which ρ is the liquid density, become sufficiently small to allow sufficient contact.[20] This, however, assumes that the impact is adequate to drive prior drainage of the intervening oil film between the marbles to allow them to be in sufficient proximity for contact in the first place. We nevertheless observe the velocity of the second marble as it drops into the collection fluid to always exceed u_c such that coalescence always occurs,

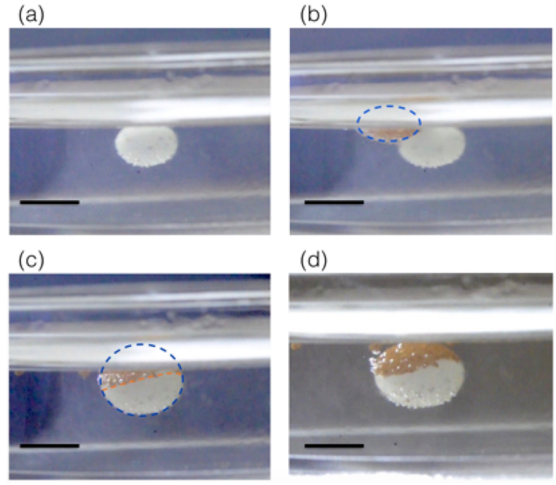

Figure 4. (a−d) Time-series images illustrating the slow coalescence of two liquid marbles to form a Janus liquid marble as a second rust-colored *Lycopodium*−iron oxide marble falls into the oil bath on the first white *Lycopodium* marble. The period between consecutive frames is 0.02 s and the scale bar denotes a length of approximately 5 mm.

provided that the both liquid marbles land at the same location in the oil bath, which is almost always ensured given that both marbles invariably drop from a fixed position dictated by the narrow slide orifice above. Unlike the banded or patchy liquid marbles that are produced in the case where $\theta < \theta_c$ in which rapid coalescence takes place as a result of the collision of the rolling second liquid marble into the stationary first marble at the slide orifice; however, the slow and controlled coalescence in the oil bath produces a symmetric Janus liquid marble with roughly a 1:1 particle ratio as observed in Figures 2c-iii and 4d.

Besides facilitating controlled and reproducible selection of these composite liquid marble morphologies (e.g., between the banded, patchy and Janus structures), another advantage of the present platform is the ability to tune the relative coverage of the particle species in the Janus marbles. Figure 2c-iv shows that a second coalescence event can be instituted in the collection fluid by dispensing a third 10 μL water droplet to form a *Lycopodium* liquid marble, which upon coalescence with the symmetric (1:1) Janus marble in the collection fluid, results in an asymmetric (1:2) Janus pattern. Further asymmetry in the particle species partitioning can then be controllably obtained with the coalescence of additional liquid marbles by sequentially adding more water droplets at the top of the slide. For example, a third coalescence event with the addition of another 10 μL water droplet (to hence produce a fourth *Lycopodium* marble) leads to a Janus liquid marble with a 1:3 coverage (Figure 2c-v). As long as the volumes of the dispensed droplets are well-controlled, fairly precise partitioning ratios can be obtained, as seen from the good agreement in the images in Figures 2c-iii−c-v between the actual particle partition delineation (interface between the white and rust colored hemispheres) obtained in the experiments with the theoretical prediction (blue dashed line), which was calculated by considering the hemispherical surface areas for a given partition ratio. Figure 5, which shows the manufacture of multiple Janus liquid marbles using this slide platform, provides the first demonstration of the possibility for rapid and continuous production of these composite liquid marbles on demand. Although we manually synthesized tens of marbles within minutes, the use of programmed automated droplet dispensers

DOI: 10.1021/acsami.6b05321
ACS Appl. Mater. Interfaces 2016, 8, 17751−17756

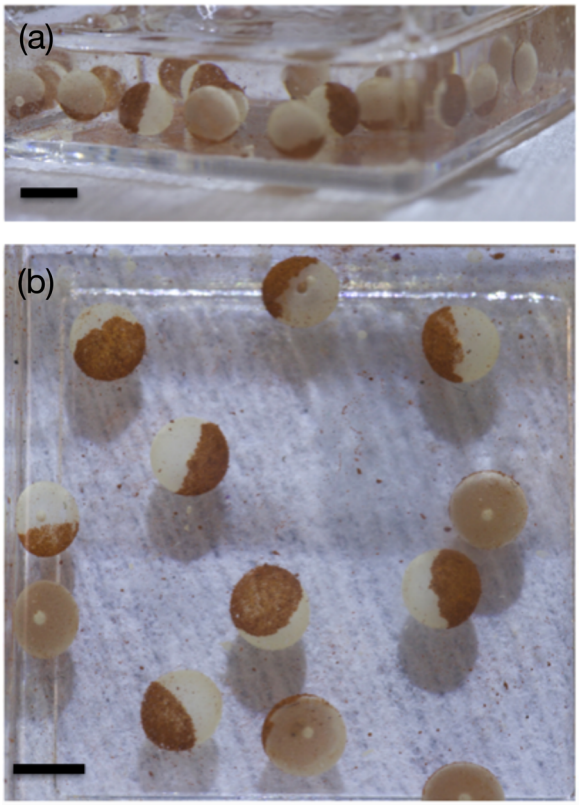

Figure 5. (a) Side and (b) top view showing the continuous successive production of multiple Janus liquid marbles using the slide platform. The scale bar denotes a length of 5 mm.

could potentially increase the production rate to hundreds of marbles per minute.

Finally, we also show a unique and simple demonstration of the possibility for noninvasive splitting of the Janus *Lycopodium* and *Lycopodium*–iron oxide liquid marble; such splitting, which allows a reduction in size and a corresponding increase in the overall surface area, can potentially improve the efficiency of liquid marbles in gas sensing[10] and microreactor[21] applications, among others. Given the magnetism of the iron oxide particles, Figure 6 shows the formation of a protrusion from the side of the liquid marble where the *Lycopodium*–iron oxide particles

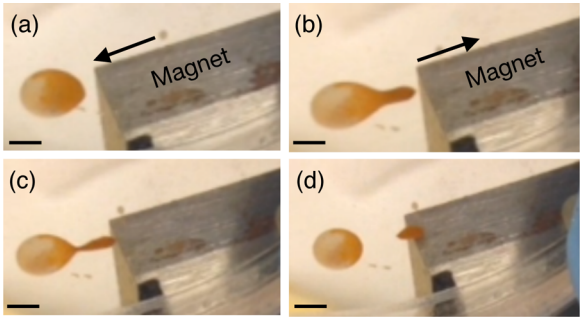

Figure 6. Sequential images showing the splitting of a Janus liquid marble to form a daughter marble when a magnet beneath the Petri dish containing the liquid marble in silicone oil is brought into proximity with the face comprising the *Lycopodium*–iron oxide coating and subsequently withdrawn. The interval between two successive images is approximately 1 s. The scale bars denote a length of approximately 2 mm.

partitioned when an underlying magnet is brought into proximity with the liquid marble. Withdrawal of the magnet in the opposite direction results in the elongation and subsequent pinch-off of the protrusion to form a daughter liquid marble comprising of *Lycopodium*–iron oxide alone. This technique overcomes limitations with other splitting processes, which typically involve invasive procedures such as dissecting a liquid marble with the use of a handheld spatula,[22] which can potentially disrupt the surface coverage of the parent liquid marble or destabilize it.

We are grateful for Prayank Gupta for initial experiments. J.C. and B.N. are grateful for CNPq (Conselho Nacional de Desenvolvimento Cientifico e Tecnologico) for providing the scholarship during the exchange and summer research. J.C. is also grateful for support from Universidade Federal do Ceara (UFC) and B.N. is grateful for support from Pontificia Universidade Catolica do Rio grande do Sul (PUCRS). A.R. is grateful for an RMIT University Vice-Chancellor's Research Fellowship. L.Y.Y. is funded through an Australian Research Council (ARC) Future Fellowship (FT130100672) as well as Discovery Project Grant DP140100805.

AUTHOR INFORMATION

Corresponding Authors

*E-mail: amgad.rezk@rmit.edu.au.
*E-mail: nicky.eshtiaghi@rmit.edu.au.

Notes

The authors declare no competing financial interest.

REFERENCES

(1) Aussillous, P.; Quéré, D. Liquid Marbles. *Nature* **2001**, *411*, 924–927.
(2) Bormashenko, E. Liquid Marbles: Properties and Applications. *Curr. Opin. Colloid Interface Sci.* **2011**, *16*, 266–271.
(3) Aussillous, P.; Quéré, D. Properties of Liquid Marbles. *Proc. R. Soc. London, Ser. A* **2006**, *462*, 973–999.
(4) Hashmi, A.; Strauss, A.; Xu, J. Freezing of a Liquid Marble. *Langmuir* **2012**, *28*, 10324–10328.
(5) Bormashenko, E.; Pogreb, R.; Whyman, G.; Musin, A.; Bormashenko, Y.; Barkay, Z. Shape, Vibrations, and Effective Surface Tension of Water Marbles. *Langmuir* **2009**, *25*, 1893–1896.
(6) Xue, Y.; Wang, H.; Zhao, Y.; Dai, L.; Feng, L.; Wang, X.; Lin, T. Magnetic Liquid Marbles: a "Precise" Miniature Reactor. *Adv. Mater.* **2010**, *22*, 4814–4818.
(7) Arbatan, T.; Li, L.; Tian, J.; Shen, W. Liquid Marbles as Microbioreactors for Rapid Blood Typing. *Adv. Healthcare Mater.* **2012**, *1*, 80–83.
(8) Vadivelu, R. K.; Ooi, C. H.; Yao, R.-Q.; Tello Velasquez, J.; Pastrana, E.; Diaz-Nido, J.; Lim, F.; Ekberg, J. A.; Nguyen, N.-T.; St John, J. A. Generation of Three-dimensional Multiple Spheroid Model of Olfactory Ensheathing Cells using Floating Liquid Marbles. *Sci. Rep.* **2015**, *5*, 15083.
(9) Bormashenko, E.; Balter, R.; Aurbach, D. Micropump based on Liquid Marbles. *Appl. Phys. Lett.* **2010**, *97*, 091908.
(10) Tian, J.; Arbatan, T.; Li, X.; Shen, W. Liquid Marble for Gas Sensing. *Chem. Commun.* **2010**, *46*, 4734–4736.
(11) Bormashenko, E.; Musin, A. Revealing of Water Surface Pollution with Liquid Marbles. *Appl. Surf. Sci.* **2009**, *255*, 6429–6431.
(12) McHale, G.; Newton, M. I. Liquid Marbles: Principles and Applications. *Soft Matter* **2011**, *7*, 5473–5481.
(13) Bormashenko, E.; Bormashenko, Y.; Pogreb, R.; Gendelman, O. Janus Droplets: Liquid Marbles Coated with Dielectric/Semiconductor Particles. *Langmuir* **2011**, *27*, 7–10.
(14) Xu, Z.; Zhao, Y.; Dai, L.; Lin, T. Multi-Responsive Janus Liquid Marbles: The Effect of Temperature and Acidic/Basic Vapors. *Part. Part. Syst. Charact.* **2014**, *31*, 839–842.

DOI: 10.1021/acsami.6b05321
ACS Appl. Mater. Interfaces 2016, 8, 17751–17756

(15) Al-Lazikani, B.; Banerji, U.; Workman, P. Combinatorial Drug Therapy for Cancer in the Post-genomic Era. *Nat. Biotechnol.* **2012**, *30*, 679−692.
(16) Zhao, Y.; Shum, H. C.; Chen, H.; Adams, L. L.; Gu, Z.; Weitz, D. A. Microfluidic Generation of Multifunctional Quantum Dot Barcode Particles. *J. Am. Chem. Soc.* **2011**, *133*, 8790−8793.
(17) Zhou, H.; Wang, H.; Niu, H.; Lin, T. Superphobicity/philicity Janus Fabrics with Switchable, Spontaneous, Directional Transport Ability to Water and Oil Fluids. *Sci. Rep.* **2013**, *3*, 2964.
(18) Ge, L.; Shao, W.; Lu, S.; Guo, R. Droplet Topology Control of Janus Emulsion prepared in One-step High Energy Mixing. *Soft Matter* **2014**, *10*, 4498−4505.
(19) Bormashenko, E.; Pogreb, R.; Balter, R.; Aharoni, H.; Bormashenko, Y.; Grynyov, R.; Mashkevych, L.; Aurbach, D.; Gendelman, O. Elastic Properties of Liquid Marbles. *Colloid Polym. Sci.* **2015**, *293*, 2157−2164.
(20) Planchette, C.; Biance, A.-L.; Pitois, O.; Lorenceau, E. Coalescence of Armored Interface under Impact. *Phys. Fluids* **2013**, *25*, 042104.
(21) Sato, E.; Yuri, M.; Fujii, S.; Nishiyama, T.; Nakamura, Y.; Horibe, H. Liquid Marbles as a Micro-reactor for Efficient Radical Alternating Copolymerization of Diene Monomer and Oxygen. *Chem. Commun.* **2015**, *51*, 17241−17244.
(22) Zhao, Y.; Fang, J.; Wang, H.; Wang, X.; Lin, T. Magnetic Liquid Marbles: Manipulation of Liquid Droplets using Highly Hydrophobic Fe_3O_4 Nanoparticles. *Adv. Mater.* **2010**, *22*, 707−710.

DOI: 10.1021/acsami.6b05321
ACS Appl. Mater. Interfaces 2016, 8, 17751−17756